Electrochemistry Communications 164 (2024) 107749

Contents lists available at ScienceDirect

Electrochemistry Communications

journal homepage: www.elsevier.com/locate/elecom

The effect of Al on the corrosion resistance of binary Mg-Al solid solutions: Combining in-situ electrochemistry with combinatorial thin films

Markus Felten [a], Alexander Lutz [a], Shamsa Aliramaji [b], Siyuan Zhang [c], Christina Scheu [c], Jochen Schneider [b], Daniela Zander [a,*]

[a] Chair of Corrosion and Corrosion Protection, RWTH Aachen University, Intzestr. 5, Aachen 52074, Germany
[b] Materials Chemistry, RWTH Aachen University, Kopernikusstr. 10, Aachen 52074, Germany
[c] Max-Planck-Institut für Eisenforschung GmbH, Düsseldorf 40237, Germany

ARTICLE INFO

Keywords:
Magnesium
Corrosion
Thin film
STEM
SVET

ABSTRACT

The effect of varying Al concentrations on the electrochemical corrosion resistance of binary Mg-Al solid solutions thin films under alkaline immersion conditions was investigated via a combination of in-situ flow-cell, scanning vibrating electrode technique and microscopy analysis. These spatially resolving characterization techniques are employed along the Al concentration gradient of the combinatorically grown thin films enabling efficient screening of the Al concentration dependent electrochemical corrosion behaviour. The analysis revealed an increasing corrosion resistance with increasing Al concentration, as a consequence of Al induced hydroxide reinforcement. Specifically, the addition of >4 wt.% Al decreases the corrosion current density in the range of 70–90 % compared to pure Mg.

1. Introduction

Magnesium (Mg) and Mg alloys represent a versatile material class for structural and functional light weight applications in the aerospace [1], medical [2–4] or energy [5,6] sector. However, the high chemical activity in conjunction with a partially protective oxide/hydroxide film leads to a low corrosion resistance under aqueous immersion conditions [7,8]. The native oxide formed in air on Mg-Al solid solutions comprises an Al-enriched Mg/MgO interface and a dense MgO layer beneath a thin plate like $Mg(OH)_2$ layer [9,10]. For Mg-Al alloys under alkaline immersion conditions (pH > 10.5) a dense $Mg(OH)_2$ layer ($Mg(OH)_{2\_dense}$) beneath a porous flake-like $Mg(OH)_2$ layer ($Mg(OH)_{2\_flake}$), was recently reported, with $Mg/Mg(OH)_{2\_dense}$ and $Mg(OH)_{2\_dense}/Mg(OH)_{2\_flake}$ interfaces enriched in Al [11]. While the $Mg(OH)_{2\_dense}$ layer tends to affect both the oxygen reduction reaction (ORR) and the hydrogen evolution reaction (HER) [11], the Al enriched interface decreases the anodic partial reaction [12–14]. Yang et al. [14] calculated an increased work function of Mg atoms in the presence of a thermodynamically preferred Al surface coverage. Thus, Al impairs the withdrawal of electrons from Mg and impedes the Mg oxidation. As reported by Nordlien et al. [12], for Al bulk concentration (c_{Al}) exceeding 4 wt.%, a continuous Al-enriched interface forms a skeletal barrier, which significantly reduces the ion flux through the oxide/hydroxide. Grimm et al. [13] reported a similar threshold for Mg-Al solid solution in the as cast condition, whereas a threshold of $c_{Al} \sim 8$ wt.% was determined in a saturated $Mg(OH)_2$ solution (pH = 10.5) after homogenization treatment. Mathieu et al. [15] determined a linear increase of the corrosion resistance with increasing c_{Al} in an ASTM D1384 electrolyte (pH = 8.3). The different conclusions might arise as a consequence of varying experimental factors: a small number of investigated specimens, c_{Al} inhomogeneities, ex-situ analysis or varying electrolyte conditions. While conventional investigations require a major experimental effort, the present study utilizes a fast-screening approach to overcome the mentioned challenges by investigating Al-graded Mg thin films with an in-situ flow-cell design and scanning vibrating electrode technique (SVET) measurements, to consistently explore the effect of Al on the corrosion resistance of Mg-Al solid solutions.

2. Material and methods

A Mg thin film (Mg_{ref}) and two binary Mg-Al thin films with different Al-gradients were synthesized. The thin film deposition was carried out by combinatorial magnetron sputtering in a high vacuum chamber using elemental targets of Mg (99.95 %), and Al (99.99 %) on d = 50.8 ± 0.3

* Corresponding author.
E-mail address: d.zander@gi.rwth-aachen.de (D. Zander).

https://doi.org/10.1016/j.elecom.2024.107749
Received 17 April 2024; Received in revised form 2 May 2024; Accepted 5 May 2024
Available online 7 May 2024

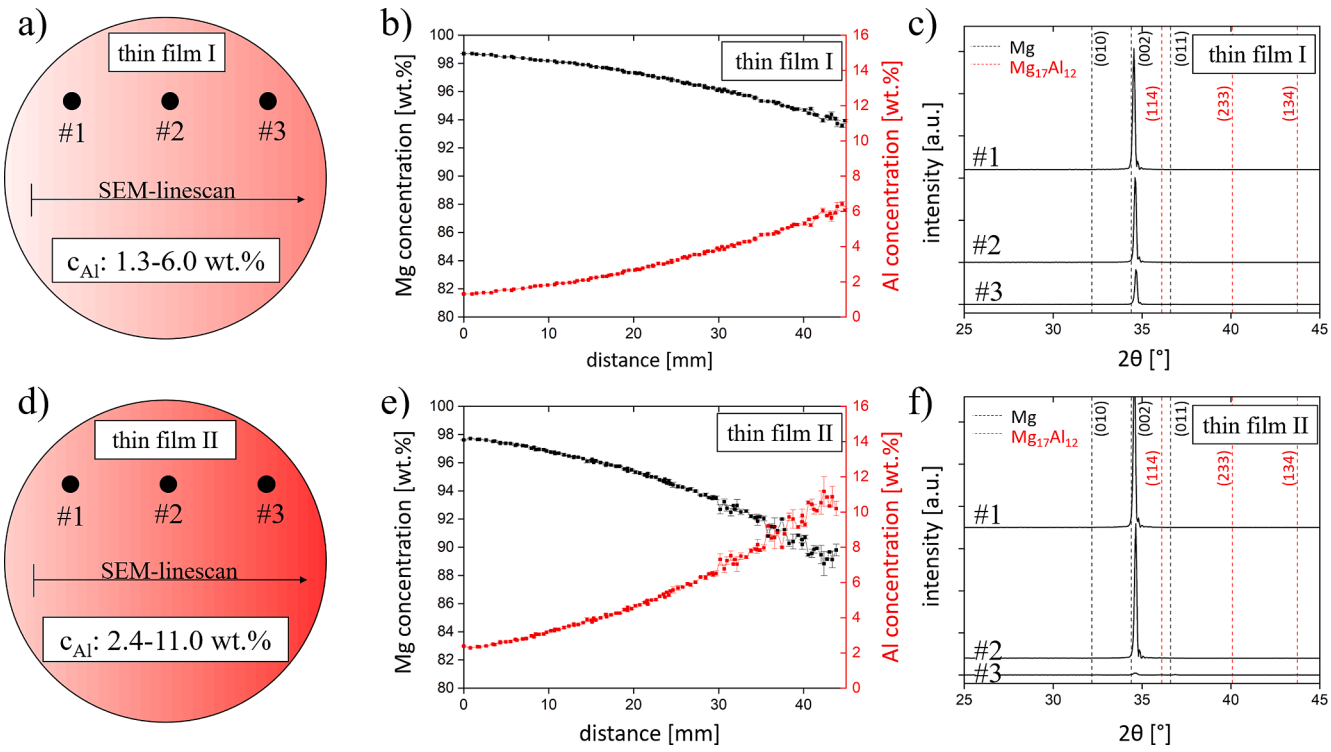

Fig. 1. Schemes, SEM/EDS and XRD measurements for the investigated binary a-c) Mg-Al thin film I and d-f) Mg-Al thin film II with an increasing Al concentration from left to right.

mm diameter Si (1 0 0) substrates at floating potential. The Mg target was powered with 200 W using RPG-50 power supply (MKS Instruments Inc., Andover, USA), whereas the Al target power was 20 and 38 W using a Maris GS 15 generator (ADL GmbH, Darmstadt, Germany). All depositions were conducted at a base pressure below 3×10^{-5} Pa, at a constant argon partial pressure of 0.5 Pa, and a substrate temperature of 100 °C. The Mg and Al targets were installed at a 45° inclination angle with respect to the substrate normal and at a 90° angle relative to each other, while the target to substrate distance equaled 10 cm. This geometric arrangement allows the formation of a compositional gradient along the substrate surface.

The Al concentration within each thin film was investigated with energy dispersive X-ray spectroscopy (EDS) in a Supra 55VP scanning electron microscope (SEM) (Carl Zeiss AG, Oberkochen, Germany). The EDS analysis was performed at an acceleration voltage of 10 kV. Spatially-resolved structural analysis of the films was performed using a Bruker D8 General Area Detection Diffraction System (XRD) (GADDS, Bruker Corporation, Billerica, MA, USA) with a Cu Kα radiation source operated at 40 kV and 40 mA. The incidence angle was fixed at 15° whereas the 2θ range was 15°-75°.

A custom built flow-cell with a specimen area of 0.03 cm^2 was manufactured by a 3D printer Form3 (Formlabs, Somerville, USA). For each thin film location along the Al gradient, the electrolyte flowed past the specimen surface at a rate of 30 ml/h for 60 min. An alkaline KOH Roti®Metic 99.98 % (Carl Roth GmbH, Karlsruhe, Germany) solution (pH = 11.5 ± 0.1) at room temperature served as the electrolyte. The dissolved ions within the electrolyte were analyzed in-situ with a NexION® 2000 inductively coupled plasma spectrometer (ICP-MS) (Perkin Elmer, Massachusetts, USA) operated in the kinetic energy discrimination mode with Ar (99.999 vol%) and He (99.9999 vol%) as the nebulizer- and the collision gas, respectively. Standard ICP multi-element solution XVI (Sigma-Aldrich, Missouri, USA) and single-element ICP-Standard-Solution-Aluminium (Carl Roth GmbH, Karlsruhe, Germany) mother solutions were diluted to Mg and Al concentrations of 1 mg/l, 0.01 mg/l and 0.001 mg/l to calibrate the ICP-MS with the same flow rate as applied on the thin films. The ion concentration in the base electrolyte was determined by applying the flow-cell setup on a Pt sheet for ~ 30 min, to subsequently correct the measured ion concentration on the Mg_{ref} and the Mg-Al thin films. The ion specific corrosion current densities ($i_{Mg,Al}$) were thereafter calculated according to Faraday's law as reported in [16]. As $i_{Mg,Al}$ values only account for dissolved ions within the electrolyte, complementary measurements are required to account for ions incorporated into the hydroxide [17,18].

Furthermore, a SVET setup manufactured by Applicable Electronics Instruments (New Haven, Connecticut, USA) and controlled by the ASET LV4 program developed by Science Wares Inc. (Falmouth, Massachusetts, USA) was utilized in a stagnant KOH electrolyte (pH_{SVET} = 12.0, ρ_{SVET} = 161 µS/cm, V_{SVET} = 1 ml) to in-situ monitor the local corrosion currents on different thin film locations for an immersion time of 60 min. A platinum black sphere with a diameter of 20 µm was electrodeposited at the tip of the Pt-Ir microelectrode, which scanned a specimen area of 0.16–0.32 mm^2 in 2–4 min at a constant height of 150 µm. The surface layer formed during the flow-cell experiments was further analyzed with scanning transmission electron microscopy (STEM) on a Titan Themis 80–300 keV microscope (Thermo Fisher Scientific, Waltham, USA) operated at 300 kV. STEM-EDS spectrum imaging was acquired using a 4-quadrant SuperX detector. Multivariate statistical analysis [19] was applied to denoise the dataset before quantification. The STEM lamella was prepared using a Scios2 focused ion beam (FIB). To protect the corrosion layers from FIB damage, C marker has been applied on the surface [20].

3. Results and discussion

Fig. 1 shows a schematic illustration of the investigated binary Mg-Al thin films with the corresponding SEM/EDS and XRD analysis. Both thin films exhibit an increasing c_{Al} (1 wt.%/cm and 1.9 wt.%/cm) and a complementary decreasing c_{Mg}. The XRD spectra in Fig. 1 c,f) show exclusively Mg (0 0 2) reflection (98–007-6748) [21], in agreement with the sharp basal-plane texture observed in other studies [22] and no

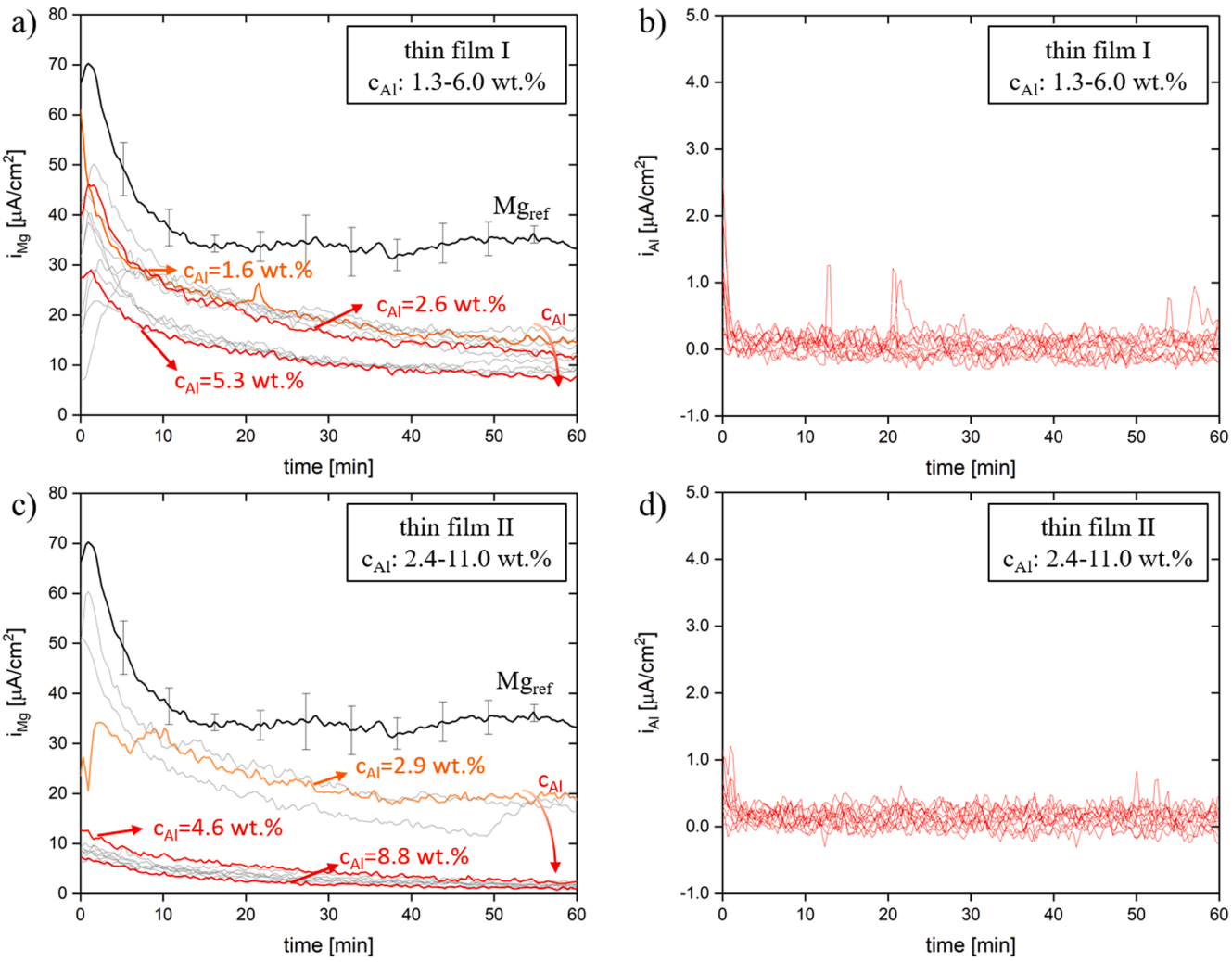

Fig. 2. In-situ corrosion current densities of the investigated binary Al-graded Mg-Al thin films. Note the increasing c_{Al} of the measurement curves from top to bottom.

further peaks.

Fig. 2 exhibits the in-situ corrosion current densities for Mg_{ref} and the binary Mg-Al thin films. A decreasing i_{Mg} over time is observed for Mg_{ref}, which reaches a dynamic equilibrium towards the final immersion time and thus indicates a surface layer formation. The same decreasing i_{Mg} trend over time is observed on both binary Mg-Al thin films. However, significantly reduced i_{Mg} values are determined on both binary Mg-Al thin films compared to Mg_{ref}. Fig. 2 b) and d) display a negligible i_{Al} ~ 0 µA/cm^2 with insignificant variation over time.

Fig. 3 shows the averaged corrosion current densities between 55–60 min in the dynamic equilibrium (i_{Mg,Al_eq}) as a function of c_{Al}. The Mg dissolution decreases with increasing c_{Al} on both binary Mg-Al thin films, leading to a decrease in the range of 70–90 % relative to pure Mg for $c_{Al} > 4$ wt.%. Furthermore, a distinct i_{Mg} decrease is observed at the reported threshold of $c_{Al} = 4$ wt.% [12] on thin film II (Fig. 3 c)). The determined i_{Al} in Fig. 3 b) and d) reveal a negligible Al dissolution into the electrolyte and indicate a potential Al incorporation in the formed surface layer. Furthermore, SVET measurements were conducted below and above $c_{Al} = 4$ wt.% to further explore the effect of Al on the passive layer formation and the corrosion resistance of binary Mg-Al solid solutions.

The SVET measurement on Mg_{ref} in Fig. 4 a) shows a large local anode-, a small local cathode- and a transition regime in between at the surface after 60 min immersion. The SVET measurements on the thin film II with $c_{Al} = 3.3$ wt.% (Fig. 4 b)) exhibit a significantly increased cathode- and transition regime instead, while Fig. 4 c) shows solely cathodic current densities for $c_{Al} = 4.8$ wt.% at the surface. Thus, while the overall ionic current densities are in a comparable range for the investigated alloys, an increasing c_{Al} enhances the cathodic current densities at the surface until exclusively cathodic current densities (HER/ORR) are detected at the threshold of c_{Al} ~ 4 wt.%. The same effect was observed on thin film I and is associated with a passive layer reinforcement due to an increasing Al incorporation in the formed hydroxide film.

The surface layer formed during the flow-cell experiments was further analyzed via STEM in Fig. 5 for a specimen with $c_{Al} = 6$ wt.%. The hydroxide comprises an inner dense $Mg(OH)_2$ layer ($Mg(OH)_{2\_dense}$) and an outer porous flake-like $Mg(OH)_2$ layer ($Mg(OH)_{2\_flake}$). While the latter precipitates from the electrolyte after exceeding the solubility limit of Mg^{2+} and OH^- [23], the $Mg(OH)_{2\_dense}$ is thermodynamically stable in alkaline electrolytes (pH > 10.5) [24]. Furthermore, Al enriched $Mg/Mg(OH)_{2\_dense}$ and $Mg(OH)_{2\_dense}/Mg(OH)_{2\_flake}$ interfaces are observed, as previously reported for a Mg-Al-Ca solid solution ($c_{Al} =$ 2 wt.%) in the same electrolyte [11]. While the latter Al enrichment stems from the native oxide, the Al concentration (Al/(Mg + Al)) > 10 %) in this case is even higher at the $Mg/Mg(OH)_{2\_dense}$ interface than reported in ref. [11]. These results confirm that the Al enrichment at the interface increases with higher c_{Al}. The assumed Al incorporation during the hydroxide layer formation (Fig. 3 b) and d)) tends to induce a preferred Al enriched $Mg/Mg(OH)_{2\_dense}$ interface. A continuous

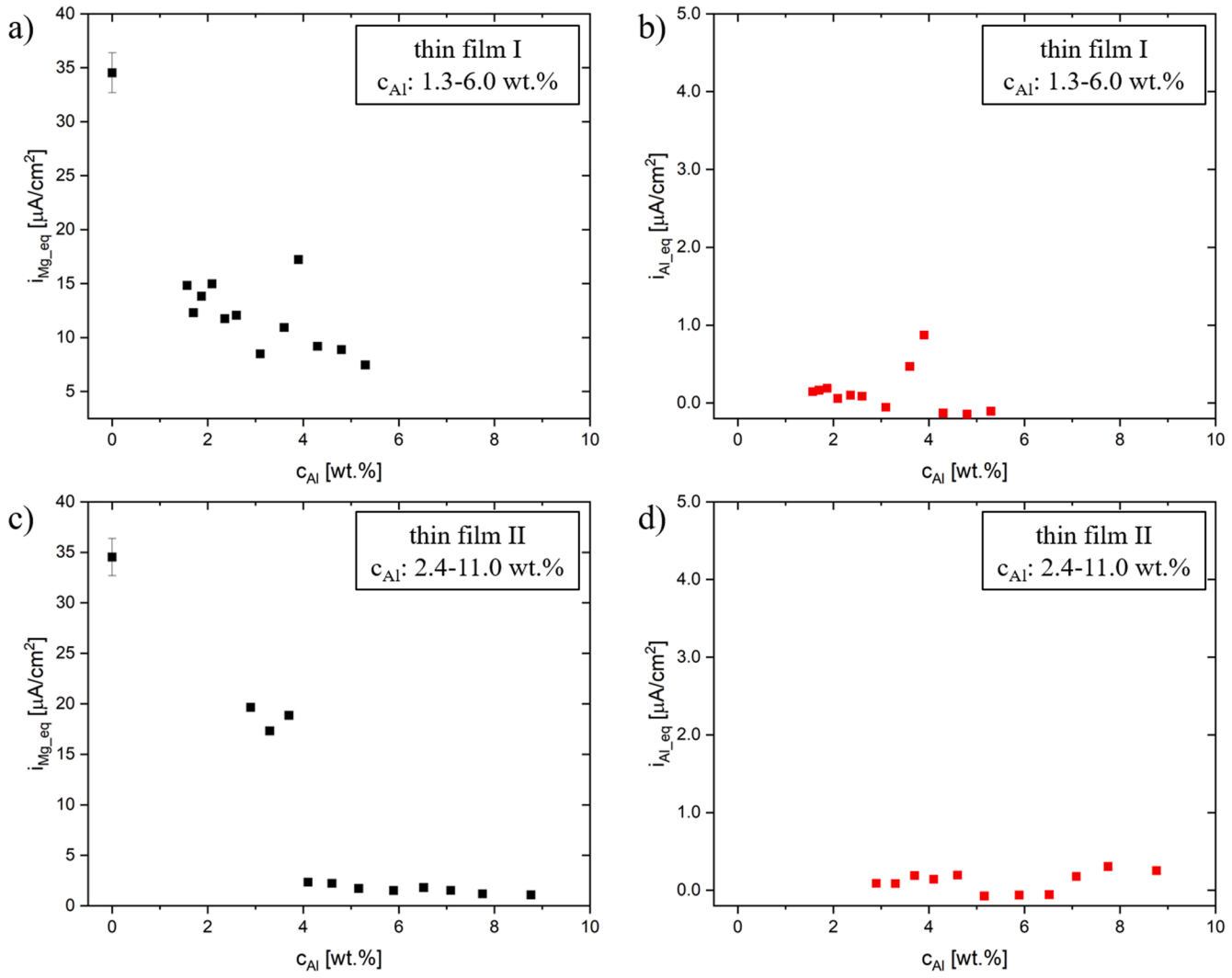

Fig. 3. Corrosion current densities in the dynamic equilibrium as a function of c_{Al}.

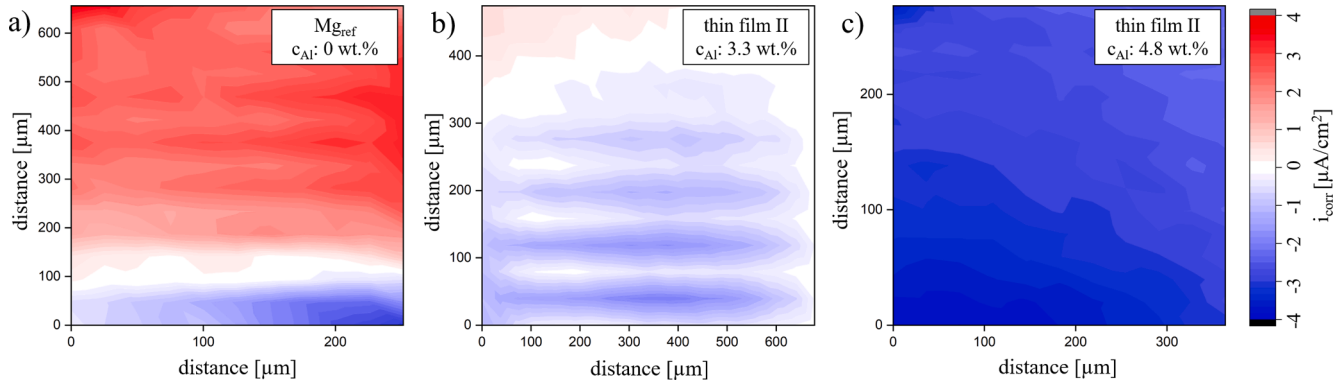

Fig. 4. SVET scans after 60 min immersion for a) Mg_{ref} as well as on thin film II with b) c_{Al} = 3.3 wt.% and c) c_{Al} = 4.8 wt.% in a KOH electrolyte (pH = 12.0).

coverage by the Al enriched Mg/$Mg(OH)_{2\_dense}$ interface is suggested at $c_{Al} > 4$ wt.%, leading to a reduced anodic Mg^{2+} ion flux through the formed $Mg(OH)_{2\_dense}$ layer and consecutively causing the distinct i_{Mg} decrease in Fig. 3 b). Thus, a predominant cathodic partial reaction occurs at the surface as shown in Fig. 4 c), to balance the anodic partial reaction below the $Mg(OH)_{2\_dense}$ layer. Fig. 5 further shows an increasing Si concentration towards the surface. Si apparently dissolves from the 3D printed flow-cell into the electrolyte at pH = 11.5. Nevertheless, Si forms soluble ions at pH = 11.5 and an electrode potential of $E = -0.99 \pm 0.1$ $V_{Hg/HgO}$, $c_{Si} < 10^{-3}$ (separately determined for c_{Al} = 1–2 wt.%) [25]. Therefore, the detected Si is a residue of the dried electrolyte on the specimen surface, as the thin films cannot be rinsed with isopropanol/distilled water after the conducted flow-cell experiment without deteriorating the surface layers.

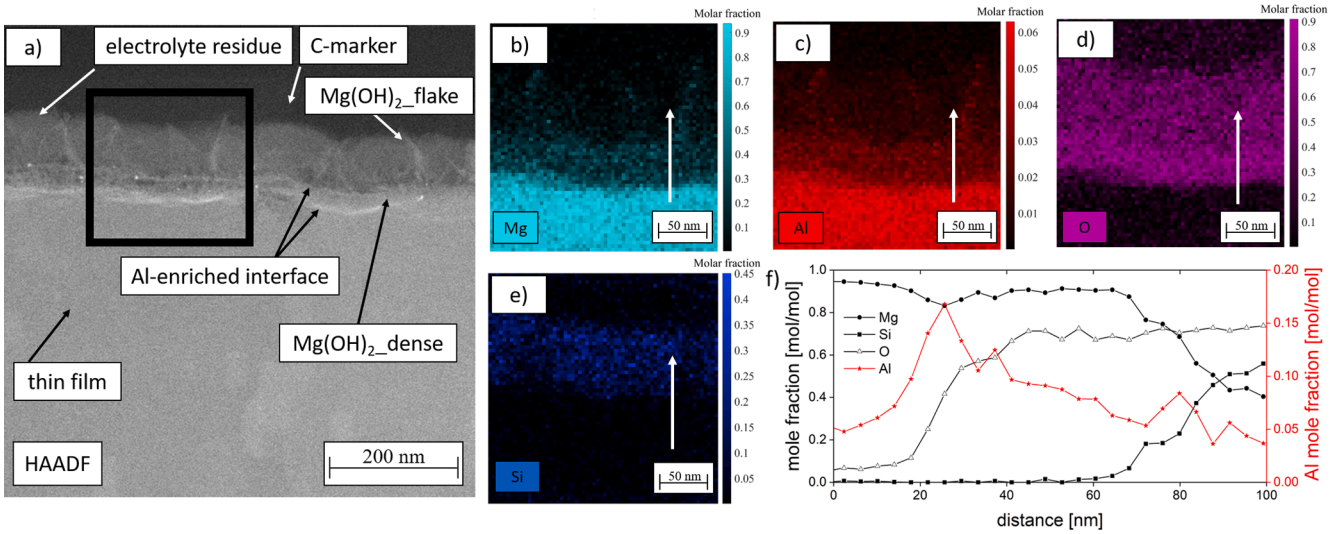

Fig. 5. STEM/EDS analysis of a Mg-Al solid solution with c_{Al} = 6 wt.% after 60 min immersion in a KOH electrolyte (pH = 11.5). a) High-angle annular dark field (HAADF)-STEM image, b-e) elemental maps and f) elemental line profile along the white arrow in b-e).

4. Conclusion

This study presents a methodology for the efficient analysis of chemical composition dependent corrosion behavior utilizing combinatorically grown thin films. We investigate the electrochemical corrosion resistance along the concentration gradient of binary Mg-Al solid solution thin films in alkaline KOH solutions by in-situ measurements of the dissolved ions with a flow-cell coupled to ICP-MS and the local corrosion current densities with SVET. The following main conclusions are obtained:

- Binary solid solution Mg-Al thin films with Al concentration gradients (1 wt.%/cm and 1.9 wt.%/cm) were synthesized to enable efficient in-situ screening of the electrochemical corrosion resistance along the gradient by probing an area of 0.03 cm^2.
- The corrosion resistance of Mg-Al solid solutions increases with the increasing Al concentration. The addition of $c_{Al} > 4$ wt.% decreases the corrosion current density in the range of 70–90 % compared to pure Mg.
- A full coverage of the Al enriched Mg/$Mg(OH)_{2\_dense}$ interface is assumed for an Al concentration of $c_{Al} \sim 4$ wt.%, which cause a reduced Mg dissolution across the hydroxide. Thus, a predominant cathodic partial reaction is established at the surface, to balance the anodic partial reaction below the $Mg(OH)_{2\_dense}$ layer.
- The hydroxide layers formed in the KOH electrolyte comprise a porous $Mg(OH)_{2\_flake}$, an inner dense $Mg(OH)_{2\_dense}$ layer and two Al enriched Mg/$Mg(OH)_{2\_dense}$- and $Mg(OH)_{2\_dense}$/ $Mg(OH)_{2\_flake}$ interfaces.

CRediT authorship contribution statement

Markus Felten: Writing – review & editing, Writing – original draft, Visualization, Validation, Methodology, Investigation, Formal analysis, Conceptualization. **Alexander Lutz:** Writing – review & editing, Investigation. **Shamsa Aliramaji:** Writing – review & editing, Investigation. **Siyuan Zhang:** Writing – review & editing, Investigation. **Christina Scheu:** Writing – review & editing, Supervision, Resources, Funding acquisition. **Jochen Schneider:** Writing – review & editing, Supervision, Resources, Funding acquisition. **Daniela Zander:** Writing – review & editing, Software, Resources, Funding acquisition.

Declaration of competing interest

The authors declare that they have no known competing financial interests or personal relationships that could have appeared to influence the work reported in this paper.

Data availability

Data will be made available on request.

Acknowledgments

The authors gratefully acknowledge the financial support of the Deutsche Forschungsgemeinschaft (DFG) of the Collaborative Research Center (CRC) 1394 “Structural and Chemical Atomic Complexity - from defect phase diagrams to material properties” – project ID 409476157 and the financial support of the project G:(DE-82)EXS-SF-OPSF596 from the DFG and the Excellence Strategy of the Federal Government and the Länder. Furthermore, the authors acknowledge the constructive and valuable discussions with René Daniel Pütz from the chair of corrosion and corrosion protection – RWTH Aachen University.

References

[1] J. Bai, Y. Yang, C. Wen, J. Chen, G. Zhou, B. Jiang, X. Peng, F. Pan, J. Magnes, Alloy 11 (2023) 3609–3619, https://doi.org/10.1016/j.jma.2023.09.015.
[2] A. Atrens, M. Liu, N.I.Z. Abidin, Mater. Sci. Eng. B 176 (2011) 1609–1636, https://doi.org/10.1016/j.mseb.2010.12.017.
[3] D. Mei, S.V. Lamaka, X. Lu, M.L. Zheludkevich, Corros. Sci. 171 (2020) 108722, https://doi.org/10.1016/j.corsci.2020.108722.
[4] D. Zander, P. Zaslansky, N.A. Zumdick, M. Felten, C. Schnatterer, V.F. Chaineux, J. U. Hammel, M. Storm, F. Wilde, C. Fleck, Adv. Eng. Mater. 23 (2021) 2100157, https://doi.org/10.1002/adem.202100157.
[5] W. Wang, J. Liu, J. Chen, W. Zhang, C. Li, Z. Shi, N. Wang, Electrochim. Acta 470 (2023) 143352, https://doi.org/10.1016/j.electacta.2023.143352.
[6] M. Deng, D. Höche, S.V. Lamaka, D. Snihirova, M.L. Zheludkevich, J. Power Sources 396 (2018) 109–118, https://doi.org/10.1016/j.jpowsour.2018.05.090.
[7] A. Atrens, G.-L. Song, Z. Shi, A. Soltan, S. Johnston, M. Dargusch, Encycl. Interfacial Chem. (2018) 515–534, https://doi.org/10.1016/B978-0-12-409547-2.13426-2.
[8] G. Song, A. Atrens, Adv. Eng. Mater. 5 (2003) 837–858, https://doi.org/10.1002/adem.200310405.
[9] D. Neuß, I.E. McCarroll, S. Zhang, E. Woods, W.J. Delis, L. Tanure, H. Springer, S. Sandlöbes, J. Yang, M. Todorova, Corros. Sci. 227 (2024) 111776, https://doi.org/10.1016/j.corsci.2023.111776.
[10] M. Felten, J. Nowak, O. Beyss, P. Grünewald, C. Motz, D. Zander, Corros. Sci. 212 (2023) 110925, https://doi.org/10.1016/j.corsci.2022.110925.

[11] M. Felten, R. Changizi, C. Scheu, M. Bruns, M. Strebl, S. Virtanen, D. Zander, Electrochem. Commun. 153 (2023) 107529, https://doi.org/10.1016/j.elecom.2023.107529.
[12] J.H. Nordlien, K. NişancioĞu, S. Ono, N. Masuko, J. Electrochem. Soc. 143 (1996) 2564, https://doi.org/10.1149/1.1837048.
[13] M. Grimm, A. Lohmüller, R.F. Singer, S. Virtanen, Corros. Sci. 155 (2019) 195–208, https://doi.org/10.1016/j.corsci.2019.04.024.
[14] J. Yang, K.S. Kumar, M. Todorova, J. Neugebauer, Phys. Rev. Mater. 7 (2023) 095802, https://doi.org/10.1103/PhysRevMaterials.7.095802.
[15] S. Mathieu, C. Rapin, J. Steinmetz, P. Steinmetz, Corros. Sci. 45 (2003) 2741–2755, https://doi.org/10.1016/S0010-938X(03)00109-4.
[16] S. Zhang, M. Rohloff, O. Kasian, A.M. Mingers, K.J. Mayrhofer, A. Fischer, C. Scheu, S. Cherevko, J. Phys. Chem. C 123 (2019) 23410–23418, https://doi.org/10.1021/acs.jpcc.9b07220.
[17] B. Dou, X. Li, J. Han, N. Birbilis, K. Ogle, Corros. Sci. 217 (2023) 111095, https://doi.org/10.1016/j.corsci.2023.111095.
[18] S. Lebouil, A. Duboin, F. Monti, P. Tabeling, P. Volovitch, K. Ogle, Electrochim. Acta 124 (2014) 176–182, https://doi.org/10.1016/j.electacta.2013.07.131.
[19] S. Zhang, C. Scheu, Microscopy 67 (2018) i133–i141, https://doi.org/10.1093/jmicro/dfx091.
[20] S. Zhang, I. Ahmet, S.-H. Kim, O. Kasian, A.M. Mingers, P. Schnell, M. Kölbach, J. Lim, A. Fischer, K.J. Mayrhofer, A.C.S. Appl, Energy Mater. 3 (2020) 9523–9527, https://doi.org/10.1021/acsaem.0c01904.
[21] M. Straumanis, J. Appl. Phys. 20 (1949) 726–734, https://doi.org/10.1063/1.1698520.
[22] S. Zhang, Z. Xie, P. Keuter, S. Ahmad, L. Abdellaoui, X. Zhou, N. Cautaerts, B. Breitbach, S. Aliramaji, S. Korte-Kerzel, Nanoscale 14 (2022) 18192–18199, https://doi.org/10.1039/D2NR05505H.
[23] J.H. Nordlien, S. Ono, N. Masuko, K. Nis, J. Electrochem. Soc. 142 (1995) 3320, https://doi.org/10.1149/1.2049981.
[24] M. Pourbaix, Atlas of electrochemical equilibria in aqueous solutions, NACE (1966).
[25] P.A. Nikolaychuk, SILICON 6 (2014) 109–116, https://doi.org/10.1007/s12633-013-9172-0.